Hindawi
Advances in Materials Science and Engineering
Volume 2019, Article ID 1612456, 7 pages
https://doi.org/10.1155/2019/1612456

Research Article

Electrocatalytic Properties of Calcium Titanate, Strontium Titanate, and Strontium Calcium Titanate Powders Synthesized by Solution Combustion Technique

Oratai Jongprateep[1,2], **Nicha Sato**[1], **Ratchatee Techapiesancharoenkij**[1,2] **and Krissada Surawathanawises**[1]

[1]*Department of Materials Engineering, Faculty of Engineering, Kasetsart University, Bangkok 10900, Thailand*
[2]*Materials Innovation Center, Faculty of Engineering, Kasetsart University, Bangkok 10900, Thailand*

Correspondence should be addressed to Oratai Jongprateep; oratai.j@ku.ac.th

Received 29 October 2018; Accepted 13 February 2019; Published 4 April 2019

Academic Editor: Alexander Kromka

Calcium titanate ($CaTiO_3$), strontium titanate ($SrTiO_3$), and strontium calcium titanate ($Sr_xCa_{1-x}TiO_3$) are widely recognized and utilized as dielectric materials. Their electrocatalytic properties, however, have not been extensively examined. The aim of this research is to explore the electrocatalytic performance of calcium titanate, strontium titanate, and strontium calcium titanate, as potential sensing materials. Experimental results revealed that $CaTiO_3$, $SrTiO_3$, and $Sr_{0.5}Ca_{0.5}TiO_3$ powders synthesized by the solution combustion technique consisted of submicrometer-sized particles with specific surface areas ranging from 4.19 to 5.98 m^2/g. Optical bandgap results indicated that while $CaTiO_3$ and $SrTiO_3$ had bandgap energies close to 3 eV, $Sr_{0.5}Ca_{0.5}TiO_3$ yielded a lower bandgap energy of 2.6 eV. Cyclic voltammetry tests, measured in 0.1 M sodium nitrite, showed oxidation peaks occurring at 0.58 V applied voltage. The highest peak current was observed in $Sr_{0.5}Ca_{0.5}TiO_3$ powder. The superior electrocatalytic performance of $Sr_{0.5}Ca_{0.5}TiO_3$ might be attributed to lower bandgap energy, which consequently facilitates higher electron transfer. Electrocatalytic performance of $Sr_{0.5}Ca_{0.5}TiO_3$ was subsequently reexamined in a wider concentration range of sodium nitrite. The results revealed that the material responded linearly to nitrite solution in the range of 0.1 mM to 0.1 M and exhibited sensitivity ranging from 3.117 to 0.040 μA/mM, in the entire tested nitrite concentrations. The results suggest that $Sr_{0.5}Ca_{0.5}TiO_3$ could also be used for nitrite detection.

1. Introduction

Calcium titanate, strontium titanate, and strontium calcium titanate are perovskite-structured ceramics often exploited in fabrication of electronic devices. In general, perovskite-structured titanate, such as $CaTiO_3$, $SrTiO_3$, $BaTiO_3$, and $FeTiO_3$, have relatively wide bandgap energies ranging between 2.8 and 3.6 eV [1–6]. Bandgap energies can be modified to suit the intended application through doping [7]. Perovskite materials, owing to their high stability, good electrical response, and bandgap energy capability to be tailored, have been developed for utilization in photocatalytic applications as in wastewater treatment, which involved antibiomicrobial action and water splitting [8–10]. Other known usages of perovskite materials include the production of solar cells and gas sensing as well as biosensing devices [11, 12]. Since nonenzymatic sensors used in food chemical or human fluid detection are generally produced from semiconductor materials with bandgap energy values ranging from 2.3 to 3.4 eV, considering perovskite's bandgap energy characteristics, the materials have great potential for electrochemical sensors [13, 14].

Food chemical contaminant and toxicants are of great importance. For example, the food additive nitrite is a commonly used chemical in curing meat and usually

found in processed foods such as sausage, bacons, and drinks. Consumption of nitrite in high concentrations can adversely affect human health. Nitrite is known as a potential carcinogenic substance [15, 16]. It has been reported that nitrite can reduce oxygen exchange in haemoglobin and oxygen-carrying capacity with adverse health effects especially in pregnant women and infants [17, 18].

Nitrite detection via the electrochemical technique using nonenzymatic sensors requires materials with high electrocatalytic activities. Enhancement of electrocatalytic activities can be achieved through chemical composition control, microstructure refining, and material electronic structure tailoring [19, 20].

Doping is one of the processes to improve perovskite's electrochemical performance through structure alteration. Distortion of the material structure often occurs as a result of the introduction of dopants into the crystal lattice sites. This is also accompanied by an increase of charged ions [21]. Microstructure control also enhances electrocatalytic activity. Fine and porous particulates with an increased surface area also create more active sites for reactions and consequently results in improved sensing performance [22, 23]. According to Zhu et al., refined microstructure also facilitates mobility of electrons between sensing materials and substance for detection [24, 25].

This study, therefore, aims at studying electrocatalytic performance of calcium titanate, strontium titanate, and strontium calcium titanate synthesized by the solution combustion technique. Relationships among chemical compositions, microstructure, bandgap energies, and electrocatalytic properties of the materials were also examined.

2. Materials and Methods

Calcium titanate, strontium titanate, and strontium calcium titanate were synthesized by the solution combustion technique. The initial reagents consisting of calcium nitrate (Deajung), strontium nitrate (Deajung), and titanium dioxide (Sigma-Aldrich) in nitric acid (Univar) were mixed to attain an aqueous solution of 0.54 M concentration. Initiation of combustion was facilitated by glycine (Deajung), which was added to the prepared aqueous solution, at a temperature of about 400°C. The powders obtained from the solution combustion process were subsequently calcined at 900°C for 3 hours.

Chemical composition and microstructural analysis of the calcined powder were conducted using an X-ray diffractometer (Philips, X'Pert) and a scanning electron microscope (FEI, Quanta 450), respectively. ImageJ software was employed in particle size analysis, whereas Brunauer–Emmett–Teller (Micrometrics, 3 Flex) was utilized in the measurement of specific surface area of the powders.

Optical bandgap energy measurement was conducted using a UV-Vis spectrophotometer (UV-1700). The measurements of optical transmission were conducted within the wavelength ranging between 300 and 900 nanometers. The value of optical bandgap is expressed as follows [26]:

$$(\alpha h\upsilon)^2 = h\upsilon - E_g\,(\alpha h\upsilon)^2 = h\upsilon - E_g, \tag{1}$$

where α is the absorption coefficient, E_g is the energy (eV), h is Planck's constant (Js), and υ is the wave frequency.

Electrocatalytic activities of the powders were determined using a Metrohm AutoLab Potentiostat (PGSTAT302N). Cyclic voltammetry technique was performed on the working electrode containing the synthesized powder and multiwalled carbon nanotube (MWCNT) within the voltage range of −0.8 to 0.8 V, at the scan rate of 0.01 V/s. Pt was used as the counterelectrode, while Ag/AgCl as the reference electrode. The working electrode was activated in 0.1 M sodium hydroxide solution. Detection of nitrite was conducted in sodium nitrite solution with the concentration range of 0.1 to 100 mM. The working electrode was prepared by mixing the synthesized powders with the multiwalled carbon nanotubes at the ratio 1 : 1 by weight and subsequently underwent the hydrothermal process at 120°C for 5 hours. The mixture was drop onto the 1 cm by 1 cm stainless steel substrate.

3. Results and Discussion

3.1. Chemical Composition. Upon calcination, the synthesized powders were tested for their chemical compositions using the X-ray diffraction technique. The Sr-Ti-O powders exhibit the peaks corresponding to strontium titanate (JCPDS 082-0230), as shown in Figure 1. For the Ca-Ti-O powders, the compositional analysis showed a single phase corresponding to calcium titanate, $CaTiO_3$ (JCPDS 082-0229). Strontium calcium titanate, $Sr_xCa_{1-x}TiO_3$ (JCPDS 089-8032), was observed in the Sr-Ca-Ti-O powders. Low intensity peaks corresponding to anatase titanium dioxide (JCPDS 084-1285) were observed in the calcium titanate and strontium calcium titanate powder.

X-ray diffraction patterns were also utilized in the semiquantitative analysis. Fraction of the main phase ($Sr_xCa_{1-x}TiO_3$ ($x = 0$, 0.5, and 1)) to the total powder content, defined as F, was determined as follows:

$$F = \frac{\left(I^{\text{pure}}/I^{\text{mix}}\right)A_{\text{impurity}}}{A_{\text{purity}} - \left(I^{\text{pure}}/I^{\text{mix}}\right)\left(A_{\text{purity}} - A_{\text{impurity}}\right)}, \tag{2}$$

where F is the weight faction of the primary phase to the total powder, I^{mix} is the integrated intensity of pure phase and secondary phase, I^{pure} is the integrated intensity of pure phase, A_{impurity} is the mass attenuation factor of titanium dioxide (anatase), and A_{purity} is the mass attenuation factor of $SrTiO_3$ or $Sr_xCa_{1-x}TiO_3$.

The semiquantitative analysis revealed that content of the secondary phase contained in the synthesized powder was minimal. The titanium dioxide present in the synthesized powder did not exceed 1.25 wt.%. The trivial quantity of the secondary phase seemed to have not contributed to significant electrocatalytic activity alterations.

3.2. Microstructure and Specific Surface Area. Particle size and morphology of the powders generally influence

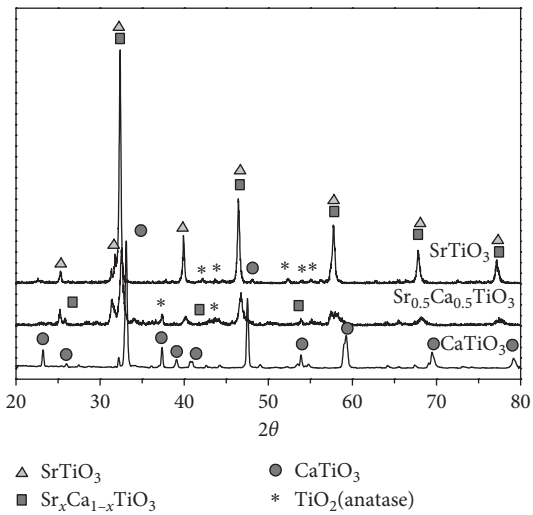

FIGURE 1: X-ray diffraction patterns of $Sr_xCa_{1-x}TiO_3$ ($x = 0$, 0.5, and 1) powders synthesized by the solution combustion technique.

specific surface area, which control reaction sites involved in the catalytic activity. In this study, the average particle sizes were determined by an image analysis technique, while the specific surface areas (SSAs) were measured by BET. Images from a scanning electron microscope revealed that the powders contained equiaxial particles with sizes in submicrometer ranges. Base on the image analysis, average particle sizes of all powders were within the range of 313 and 358 nm (Figure 2). Assuming that the particles are well dispersed, nonporous, and spherical in shape, the relationship between specific surface area and particle size can be expressed by the following equation [27]:

$$D = \frac{6}{(\rho * \mathrm{SSA})}, \tag{3}$$

where D is the average particle diameter, ρ is the density of powder, and SSA is the specific surface area.

Using equation (3), the specific surface area of the powders base on the particle size obtained from image analysis ranging would be in the range between 2.76 and 4.40 m^2/g for particle sizes ranging from 313 to 358 nm. However, in this study, specific surface area of the powders measured by the BET technique ranged from 4.19 to 5.98 m^2/g (Table 1). The marginally higher specific surface areas obtained from measurements indicated that the particles might be slightly porous in nature, which is a common observation in powders synthesized by the solution combustion technique [28, 29].

3.3. Optical Bandgap. Results from bandgap energy measurements, as shown in the tauc plot in Figure 3, indicated that bandgap energies of synthesized powders ranged between 2.59 and 3.01 eV, with the lowest values found in $Sr_{0.5}Ca_{0.5}TiO_3$. The bandgap energies of $CaTiO_3$ and $SrTiO_3$ are in close proximity, with the value of around 3 eV (Table 2). The values obtained in this study were comparable with those reported by Osterloh and Alammar et al. [30, 31].

In general, doping introduces extra energy levels between the bandgap of the host. This resulted in the decrease of total bandgap energy [32]. In this study, the combination of Sr and Ca created an impure energy band, leading to the reduction of bandgap energy. The findings were being in agreement with the results reported by Wu et al., which indicated that doping perovskite-structured metal titanate by ions of strontium, barium, and calcium facilitated minimization of bandgap energy [33].

3.4. Electrocatalytic Activity. Cyclic voltammetry was employed in the determination of electrocatalytic activities of the powders. Oxidation peaks occurring as a result of the MWCNT reaction were evident at 0.18 V, while oxidation peaks resulting from the reaction between powder and nitrite occurred at 0.58 V (Figure 4). MWCNT oxidation peaks obtained in the study were comparable with those reported by Fayemi et al. [34].

Potential oxidation reactions are expressed by the following equations:

$$Sr_{0.5}Ca_{0.5}TiO_3 + O^- + H_2O \longrightarrow Sr_{0.5}Ca_{0.5}TiO_3 + 2OH^- \tag{4}$$

$$Sr_{0.5}Ca_{0.5}TiO_3 - 2OH^- + Sr_{0.5}Ca_{0.5}TiO_3NO_2^- \longrightarrow Sr_{0.5}Ca_{0.5}TiO_3 + NO_3^- + 2e^- + H_2O \tag{5}$$

Yatsunami et al. reported a similar observation indicating that detection of nitrite can be achieved using perovskite-structured oxides such as $SmBO_3$ (B = Cr, Mn, Fe, and Co) as sensing materials [35].

In this study, oxidation peak currents ranged from 0.038 to 0.081 mA, with the greatest values found in $Sr_{0.5}Ca_{0.5}TiO_3$. Enhanced electrocatalytic activity was attributed to low bandgap energy. Narrow bandgap facilitates generation of electrical charge carriers, which consequently results in current enhancement.

Voltammetry measurements of $Sr_{0.5}Ca_{0.5}TiO_3$ were also performed in a wider concentration range of sodium nitrite. Current densities resulting from the reaction between powder and nitrite are plotted against concentration of sodium nitrite (Figure 5). Measured oxidation current densities were taken in the range between 0.1 mM and 0.1 M. Calibration curves show linear relationship between current density (J) and nitrite concentration (C) for various nitrite concentration ranges: 0.1–1 mM, 1–10 mM, and 10–100 mM, as shown in Figure 6. Fairly good linearity, represented by high R^2 values, was evident. R^2 values obtained from the current experiment ranged from 0.94 to 0.96, which were far higher than the generally accepted value of 0.75 [36].

Sensitivities of the detection are generally determined from the slope of the calibration curve. The equations representing the linear relationship and sensitivity are shown in Table 3. The sensitivity values obtained in this study were in the range between 3.12 and 0.04 $\mu A \cdot M^{-1} \cdot cm^{-2}$,

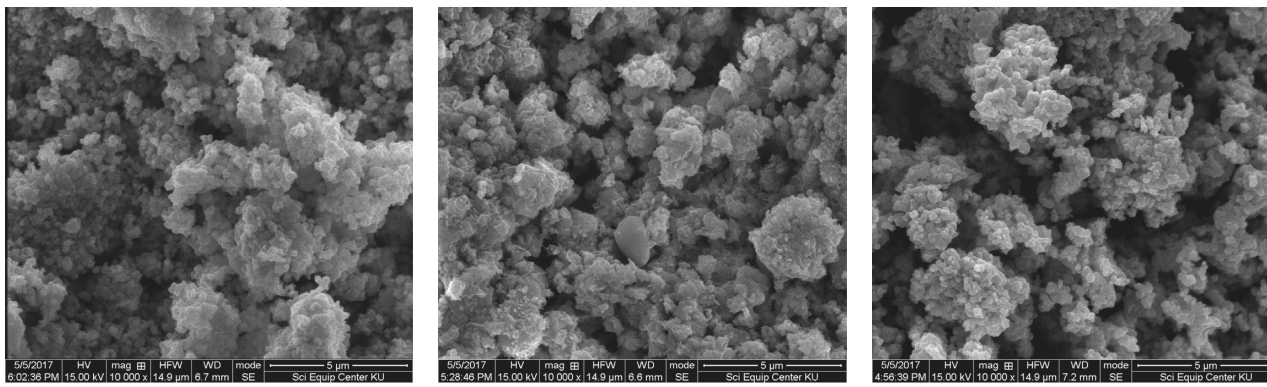

(a) (b) (c)

Figure 2: Scanning electron micrographs showing particle morphology of powders synthesized by the solution combustion technique with following compositions: (a) $CaTiO_3$; (b) $Sr_xCa_{1-x}TiO_3$; (c) $SrTiO_3$.

Table 1: The relationship of particle sizes and specific surface area.

Composition	Particle sizes (nm) ImageJ	SSA (m^2/g) BET
$CaTiO_3$	342 ± 113	5.99
$Sr_{0.5}Ca_{0.5}TiO_3$	313 ± 84	5.47
$SrTiO_3$	358 ± 91	4.19

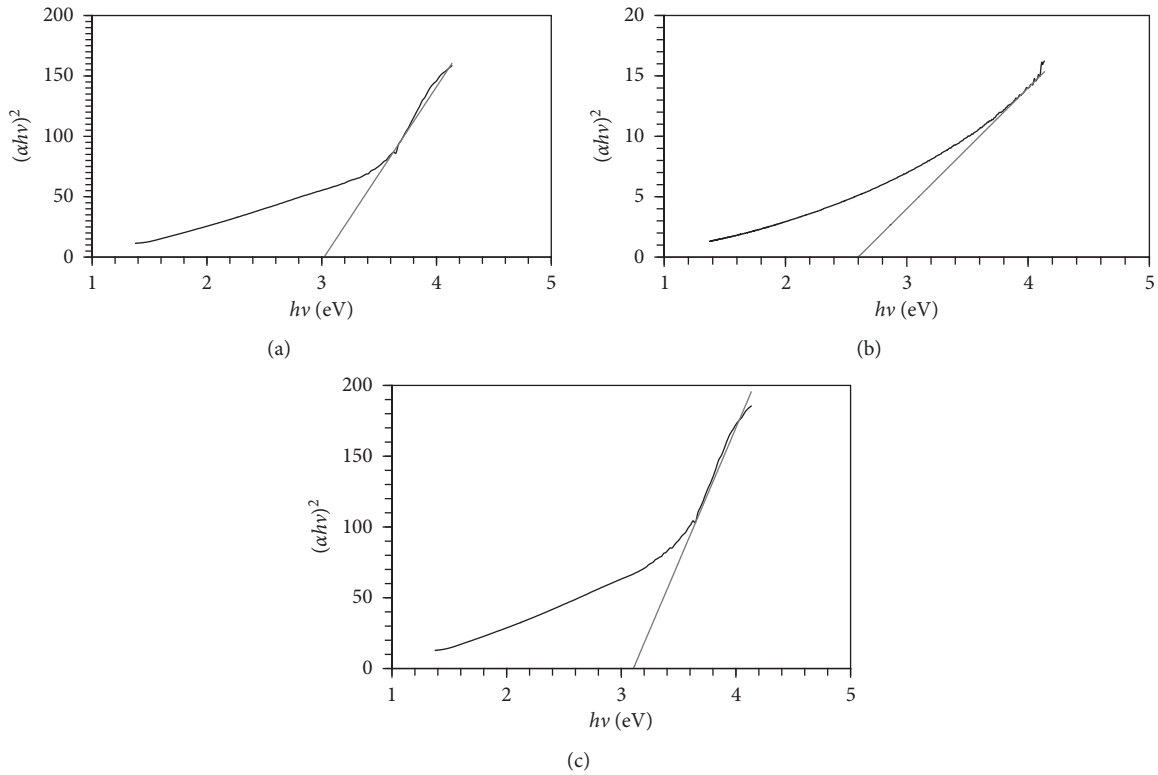

Figure 3: Tauc plot of synthesized powders with following composition: (a) $CaTiO_3$; (b) $Sr_{0.5}$ $Ca_{0.5}$ TiO_3; (c) $SrTiO_3$.

which were in the same range with the value observed by Salimi et al. The overall results, hence, suggested that that $Sr_{0.5}Ca_{0.5}TiO_3$ had potential as a nitrite detection material [37].

4. Conclusions

Calcium titanate, strontium titanate, and strontium calcium titanate powders were successfully synthesized by the

Table 2: Bandgap energy of strontium calcium titanate.

Composition	Bandgap energy (eV)
$CaTiO_3$	3.01
$Sr_{0.5}$ $Ca_{0.5}$ TiO_3	2.59
$SrTiO_3$	2.96

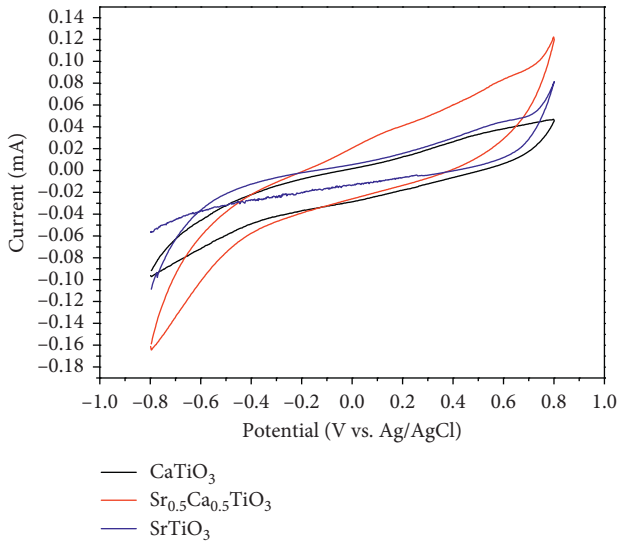

Figure 4: Voltammograms of $Sr_xCa_{1-x}TiO_3$ ($x = 0$, 0.5, and 1) in 0.1 M sodium nitrite at a scan rate of 0.01 V/s.

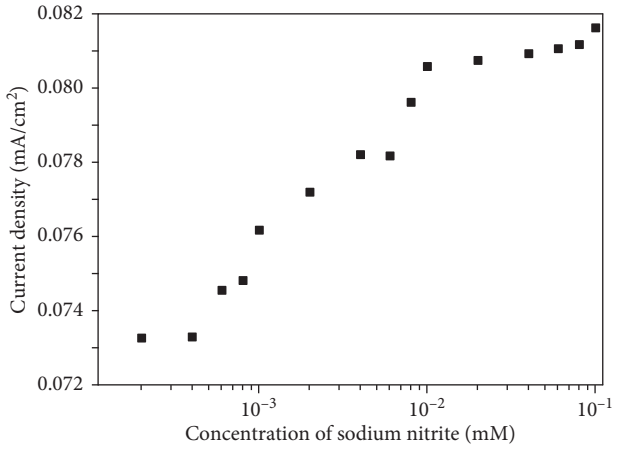

Figure 5: Calibration curve for current density vs. concentration of sodium nitrite with a working potential of 0.58 V for $Sr_xCa_{1-x}TiO_3$ ($x = 0$, 0.5, and 1) measured in the range of 0.1–100 mM.

solution combustion technique. The effects of chemical compositions on microstructure, bandgap energies, and electrocatalytic properties of the synthesized powders were examined. It was found that particle size and specific surface areas were not significantly affected by chemical compositions. However, bandgap energy was significantly reduced in strontium calcium titanate. The reduced bandgap energy contributed to enhanced electrocatalytic activity. At the applied voltage close to 0.6 V, the oxidation reaction between synthesized particles and nitrite occurred, revealing the

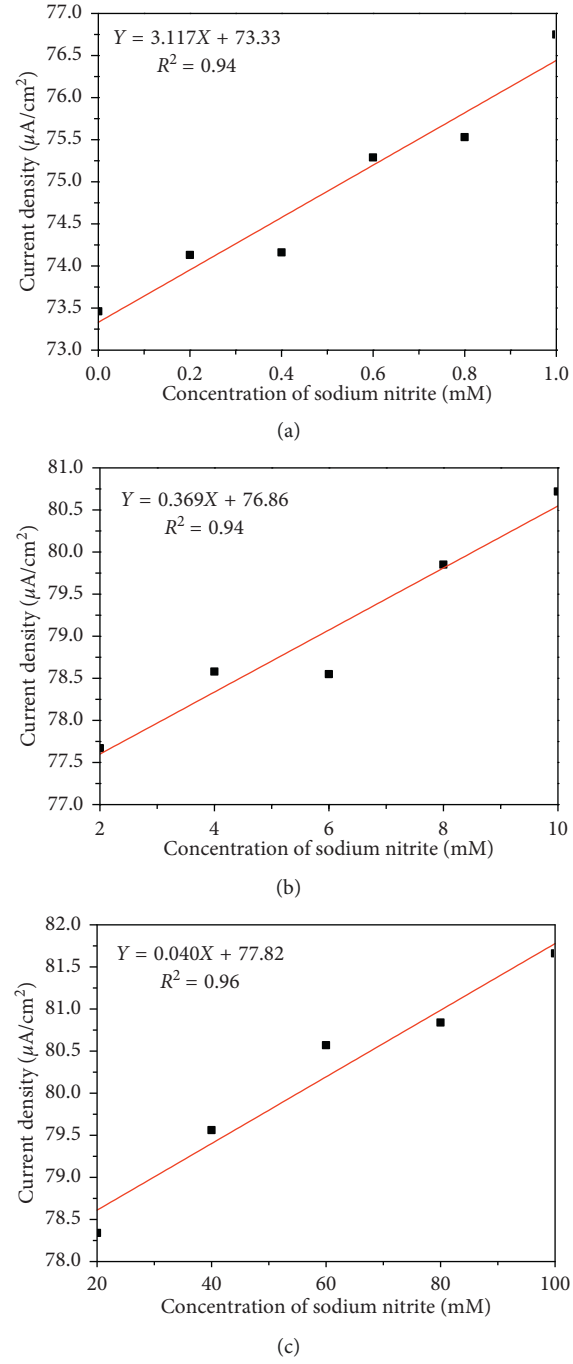

Figure 6: Calibration curves for current density vs. concentration of sodium nitrite with a working potential of 0.58 V for $Sr_xCa_{1-x}TiO_3$ ($x = 0$, 0.5, and 1), measured in the range of (a) 0.1–1 mM, (b) 1–10 mM, and (c) 10–100 mM.

Table 3: Sensitivity of $Sr_xCa_{1-x}TiO_3$ ($x = 0$, 0.5, and 1) when measured in sodium nitrite solution.

Concentration of sodium nitrite (mM)	Equations representing current density (J)	R^2	Sensitivity ($\mu A \cdot mM^{-1} \cdot cm^{-2}$)
0.1–1	$J = 3.117C + 73.33$	0.94	3.117
1–10	$J = 0.369C + 76.86$	0.94	0.369
10–100	$J = 0.040C + 77.82$	0.96	0.040

potential capability of the materials for exploitation in the fabrication of enzyme-less sensors for nitrite detection.

Data Availability

The data used to support the findings of this study are included within the article.

Conflicts of Interest

The authors declare that they have no conflicts of interest.

Acknowledgments

The authors gratefully acknowledge the financial support of Kasetsart University Research and Development Institute (KURDI), the equipment support of the KU Department of Materials Engineering, and the valuable and fruitful dialogues and suggestions of Dr. Gasidit Panomsuwan.

References

[1] E. Grabowska, "Selected perovskite oxides: characterization, preparation and photocatalytic properties-A review," *Applied Catalysis B: Environmental*, vol. 186, pp. 97–126, 2016.

[2] M. Enhessari and A. Salehabadi, "Perovskites-based nanomaterials for chemical sensors," in *Progresses in Chemical Sensor*, A. Salehabadi and W. Wang, Eds., pp. 59–91, InTechOpen, London, UK, 2016.

[3] P. Kanhere and Z. Chen, "A review on visible light active perovskite-based photocatalysts," *Molecules*, vol. 19, no. 12, pp. 19995–20022, 2014.

[4] B. Luo, X. Wang, E. Tian et al., "Electronic structure, optical and dielectric properties of $BaTiO_3/CaTiO_3/SrTiO_3$ ferroelectric superlattices from first-principles calculations," *Journal of Materials Chemistry C*, vol. 3, no. 3, pp. 8625–8633, 2015.

[5] W. Zhao, W. Zhao, G. Zhu, T. Lin, F. Xu, and F. Huang, "Black strontium titanate nanocrystals of enhanced solar absorption for photocatalysis," *CrystEngComm*, vol. 17, no. 39, pp. 7528–7534, 2015.

[6] S. Upadhyay, J. Shrivastava, A. Solanki et al., "Enhanced photoelectrochemical response of $BaTiO_3$ with Fe doping: experiments and first-principles analysis," *The Journal of Physical Chemistry C*, vol. 115, no. 49, pp. 24373–24380, 2011.

[7] M. Pazoki, T. J. Jacobsson, A. Hagfeldt et al., "Effect of metal cation replacement on the electronic structure of metal-organic halide perovskites: replacement of lead with alkaline-earth metals," *Physical Review B: Condensed Matter*, vol. 93, no. 14, 2016.

[8] X.-j. Huang, X. Yan, H.-y. Wu et al., "Preparation of Zr-doped $CaTiO_3$ with enhanced charge separation efficiency and photocatalytic activity," *Transactions of Nonferrous Metals Society of China*, vol. 26, no. 2, pp. 464–471, 2016.

[9] H. Mizoguchi, K. Ueda, M. Orita et al., "Decomposition of water by a $CaTiO_3$ photocatalyst under UV light irradiation," *Materials Research Bulletin*, vol. 37, no. 15, pp. 2401–2406, 2002.

[10] T. K. Townsend, N. D. Browning, and F. E. Osterloh, "Nanoscale strontium titanate photocatalysts for overall water splitting," *ACS Nano*, vol. 6, no. 8, pp. 7420–7426, 2012.

[11] L. Wang, J. Li, M. Feng et al., "Perovskite-type calcium titanate nanoparticles as novel matrix for designing sensitive electrochemical biosensing," *Biosensors and Bioelectronics*, vol. 96, pp. 220–226, 2017.

[12] V. Železný, D. Chvostová, L. Pajasová et al., "Temperature dependence of the optical properties of $Ba_{0.75}Sr_{0.25}$ TiO_3 thin films," *Thin Solid Films*, vol. 571, pp. 416–419, 2014.

[13] J. Tang, J. Li, P. Da, Y. Wang, and G. Zheng, "Solar-energy-driven photoelectrochemical biosensing using TiO_2Nanowires," *Chemistry-A European Journal*, vol. 21, no. 32, pp. 11288–11299, 2015.

[14] Z. Kang, X. Yan, Y. Wang et al., "Electronic structure engineering of Cu_2O film/ZnO nanorods array all-oxide p-n heterostructure for enhanced photoelectrochemical property and self-powered Biosensing application," *Scientific Reports*, vol. 5, no. 1, pp. 1–7, 2015.

[15] Y.-S. Nam, K.-C. Noh, N.-K. Kim, Y. Lee, H.-K. Park, and K.-B. Lee, "Sensitive and selective determination of ion in aqueous samples using modified gold nanoparticle as a colorimetric probe," *Talanta*, vol. 125, no. 2, pp. 153–158, 2014.

[16] M. Shivakumar, K. L. Nagashree, S. Manjappa, and M. S. Dharmaprakash, "Electrochemical detection of nitrite using glassy carbon electrode modified with silver nanospheres (AgNS) obtained by green synthesis using pre-hydrolysed liquor," *Electroanalysis*, vol. 29, no. 5, pp. 1434–1442, 2017.

[17] L. Knobeloch, B. Salna, A. Hogan, J. Postle, and H. Anderson, "Blue babies and nitrate-contaminated well water," *Environmental Health Perspectives*, vol. 108, no. 7, pp. 675–678, 2000.

[18] F. R. Greer and M. Shannon, "Infant methemoglobinemia: the role of dietary nitrate in food and water," *Pediatrics*, vol. 116, no. 3, pp. 784–786, 2005.

[19] J. W. Fergus, "Perovskite oxides for semiconductor-based gas sensors," *Sensors and Actuators B: Chemical*, vol. 123, no. 2, pp. 1169–1179, 2007.

[20] O. Jongprateep, R. Techapiesarnchareonkij, K. Surawathanawises et al., "Solution combustion route for synthesizing Co_3O_4/MWCNTs and Mn_2O_3/MWCNTs electrodes as glucose sensors," *Materials Today: Proceedings*, vol. 5, no. 5, pp. 10946–10953, 2018.

[21] N. F. Atta, A. Galal, and E. H. El-Ads, "Perovskite nanomaterials–synthesis, characterization, and applications," in *Perovskite Materials*, L. Pan, Ed., pp. 107–151, InTechOpen, London, UK, 2016.

[22] J. Peña-Bahamonde, H. N. Nguyen, S. K. Fanourakis et al., "Recent advances in graphene-based biosensor technology with applications in life sciences," *Journal of Nanobiotechnology*, vol. 16, no. 1, pp. 1–17, 2018.

[23] A. Galal, N. F. Atta, and S. M. Ali, "Investigation of the catalytic activity of $LaBO_3$ (B=Ni, Co, Fe or Mn) prepared by the microwave-assisted method for hydrogen evolution in acidic medium," *Electrochimica Acta*, vol. 56, no. 16, pp. 5722–5730, 2011.

[24] C. Zhu, G. Yang, H. Li, D. Du, and Y. Lin, "Electrochemical sensors and biosensors based on nanomaterials and nanostructures," *Analytical Chemistry*, vol. 87, no. 1, pp. 230–249, 2015.

[25] R. S. Freire, C. A. Pessoa, L. D. Mello, and L. T. Kubota, "Direct electron transfer: an approach for electrochemical biosensors with higher selectivity and sensitivity," *Journal of the Brazilian Chemical Society*, vol. 14, no. 2, pp. 230–243, 2003.

[26] C. R. Gautam, S. Das, S. S. Gautam, A. Madheshiya, and A. K. Singh, "Processing and optical characterization of lead calcium titanate borosilicate glass doped with germanium,"

Journal of Physics and Chemistry of Solids, vol. 115, pp. 180–186, 2018.

[27] E. Suito, M. Arakawa, and T. Arakawa, "Surface area measurement of powder by absorption in liquid phase. (I): calculation of specific surface area of calcium carbonate powders from the absorption of stearic acid," *Bulletin of the Institute for Chemical Research, Kyoto University*, vol. 33, no. 1, pp. 1–7, 1955.

[28] K. Manjunath and C. G. Thimmanna, "Studies on synthesis, characterization and applications of nano $CaTiO_3$ powder," *Current Nanomaterials*, vol. 1, no. 2, pp. 145–155, 2016.

[29] H. Parnianfar, S. M. Masoudpanah, S. Alamolhoda, and H. Fathi, "Mixture of fuels for solution combustion synthesis of porous Fe_3O_4 powders," *Journal of Magnetism and Magnetic Materials*, vol. 432, pp. 24–29, 2017.

[30] F. E. Osterloh, "Inorganic nanostructures for photoelectrochemical and photocatalytic water splitting," *Chemical Society Reviews*, vol. 42, no. 6, pp. 2294–2320, 2013.

[31] T. Alammar, I. Hamm, M. Wark, and A.-V. Mudring, "Low-temperature route to metal titanate perovskite nanoparticles for photocatalytic applications," *Applied Catalysis B: Environmental*, vol. 178, pp. 20–28, 2015.

[32] A. N. Andriotis and M. Menon, "Band Gap engineering via doping: a predictive approach," *Journal of Applied Physics*, vol. 117, no. 12, pp. 1–9, 2015.

[33] M. C. Wu, W. C. Chen, S. H. Chan et al., "The effect of strontium and barium doping on perovskite-structured energy materials for photovoltaic applications," *Applied Surface Science*, Vol. 429, pp. 9–15, 2018.

[34] O. E. Fayemi, A. S. Adekunle, and E. E. Ebenso, "Metal oxide nanoparticles/multi-walled carbon nanotube nanocomposite modified electrode for the detection of dopamine: comparative electrochemical study," *Journal of Biosensors & Bioelectronics*, vol. 6, no. 4, pp. 1–14, 2015.

[35] T. Yatsunami, S. Takase, and Y. Shimiz, "Amperometric nitrite-ion sensor based on electrodeposited Sm-based perovskite-type oxide thick-film electrode," *Sensors and Materials*, vol. 28, no. 7, pp. 777–784, 2016.

[36] C. Neville, C. Ludlow, and B. Rieger, "Measuring postural stability with an inertial sensor: validity and sensitivity," *Medical Devices: Evidence and Research*, vol. 8, pp. 447–455, 2015.

[37] A. Salimi, A. Noorbakhsh, and M. Ghadermarzi, "Amperometric detection of nitrite, iodate and periodate at glassy carbon electrode modified with catalase and multi-wall carbon nanotubes," *Sensors and Actuators B: Chemical*, vol. 123, no. 1, pp. 530–537, 2007.